THE ASTROPHYSICAL JOURNAL, 299:821–827, 1985 December 15

EINSTEIN OBSERVATIONS OF THE VELA SUPERNOVA REMNANT: THE SPATIAL STRUCTURE OF THE HOT EMITTING GAS

STEVEN M. KAHN
Department of Physics, University of California, Berkeley

AND

P. GORENSTEIN, F. R. HARNDEN, JR., AND F. D. SEWARD
Harvard-Smithsonian Center for Astrophysics
Received 1985 February 4; accepted 1985 June 5

ABSTRACT

Spatially resolved ($\sim 1'$) X-ray maps of the Vela supernova remnant have been constructed in two spectral bands, 0.2–1.0 keV and 0.8–2.0 keV, from a series of 36 separate observations with the Imaging Proportional Counter of the *Einstein Observatory*. The maps exhibit substantial structure on all angular scales. Spectral analysis shows that the emission from the remnant can be consistently described as thermal radiation from hot gas which is nonuniform in density and temperature, but which is in approximate pressure equilibrium. We find $p/k \approx 3\text{–}4 \times 10^5$ cm^{-3} K. The soft X-ray emission exhibits a high degree of correlation with the optical filamentary structure in the sense that the most prominent filaments either tightly surround or are coincident with the brightest X-ray regions. This suggests that the softest X-radiation may originate in "warm" gas which is evaporated from the denser clouds responsible for the optical and ultraviolet filaments. We investigate such an interpretation quantitatively and show that it is only marginally consistent with the observations.

Subject headings: nebulae: individual — nebulae: supernova remnants — X-rays: sources — X-rays: spectra

I. INTRODUCTION

The Vela and Cygnus Loop supernova remnants (SNRs) are the two most prominent examples of intermediate-age remnants in our Galaxy. Both are also bright sources in the radio, optical, and soft X-ray bands, and consequently, they have been studied extensively. The two are quite similar in size (radius ~ 20 pc), X-ray spectrum (temperature $\sim 2\text{–}4 \times 10^6$ K), X-ray luminosity (a few times 10^{35} ergs s^{-1}), and the inferred characteristics (age $\sim 1\text{–}2 \times 10^4$ yr; explosion energy a few times 10^{50} ergs; ambient density ~ 0.1 cm^{-3}) of the SN event (see review by Culhane 1977). However, they differ significantly in their overall morphological appearance. Whereas the Cygnus Loop exhibits a clear limb-brightened shell in the radio and in its optical filaments, the structure of the Vela SNR is irregular and disordered. The filaments are "wispy," less prominent than those of the Cygnus Loop, and they form what appear to be small circular shells and arches in the interior of the remnant (Miller 1973). Van den Bergh (1978) has classified Vela as a "smoke ring" remnant along with Shajn 147, which has a similar appearance. The velocity structure of the filamentary gas is also chaotic. In particular, Jenkins, Wallerstein, and Silk (1984) have produced a crude velocity map by looking at high-velocity components of absorption lines toward stars lying within or behind the remnant. They do not find higher projected radial velocities toward the center, as would be expected if the filamentary gas were moving outward from the site of the initial explosion. Instead, the highest velocity components are distributed essentially randomly within the remnant. Understanding such morphological peculiarities (particularly in relation to the Cygnus Loop) is a major problem for research on the Vela SNR and on the evolution of older remnants in general.

The Vela SNR has been observed in soft X-rays by a number of collimated proportional counter experiments. The total flux in the 0.15–2 keV band is $1.3 \pm 0.2 \times 10^{-8}$ ergs cm^{-2} s^{-1} keV^{-1} which, at a distance of ~ 500 pc, implies a luminosity of $\sim 3 \times 10^{35}$ ergs s^{-1} (Moore and Garmire 1975). A high statistical quality spectrum of the whole remnant, presented by Kahn *et al.* (1983), exhibits the presence of line emission associated with O VII and O VIII ions, which proves that most of the emission is thermal radiation produced by hot gas, presumably associated with the blast wave. The characteristic X-ray temperature is $\sim 2.4 \times 10^6$ K, although the spectra exhibit some evidence for an additional harder component with a temperature $\sim 2 \times 10^7$ K. X-ray maps of the remnant have been derived from scanning observations by Seward *et al.* (1971), Gorenstein, Harnden, and Tucker (1974), Moore and Garmire (1975), and Hearn, Larsen, and Richardson (1980). These show that the emission is most prominent in the northwest and southeast quadrants of the remnant where the filamentary structure is also pronounced, but the spatial resolution of the maps ($\sim 1°$) is not sufficient to investigate the relationship between the X-ray and optical emission in any detail. Evidence for an additional point source of hard X-ray emission coincident with the Vela pulsar, PSR 0833-45, was first reported by Harnden and Gorenstein (1973) and has since been confirmed by others (e.g., Kellogg *et al.* 1973; Culhane *et al.* 1974).

Here, we present the first spatially resolved ($\sim 1'$) map of the soft X-ray emission from the Vela SNR compiled from a series of imaging observations with the *Einstein Observatory* (Giacconi *et al.* 1979). The data show that the X-ray structure is quite complex and exhibits (in places) a correlation with the chaotic filamentary pattern. Such a correlation suggests that the bulk of the X-radiation may originate in gas produced by evaporation of denser clouds which contain the slower shocks responsible for the optical and ultraviolet filaments (McKee and Cowie 1975, 1977). We analyze the X-ray spectrum as a function of position within the remnant and determine the

temperature and pressure of the emitting gas in order to test this scenario quantitatively. In this paper, we concentrate on the thermal emission characteristic of the remnant as a whole. In a companion paper (Harnden *et al.* 1985, hereafter Paper II), we focus on the Vela pulsar and the nonthermal emission from its vicinity.

II. OBSERVATIONS AND ANALYSIS

The observations were performed with the imaging proportional counter (IPC) of the *Einstein Observatory*. This instrument is sensitive in the range 0.15–4.5 keV, has a spatial resolution $\sim 1'.5$ (FWHM) averaged over a 1 deg^2 field of view, and has a spectral resolution $\Delta E/E \approx 100\%$ at 1 keV (see Gorenstein, Harnden, and Fabricant 1981 for detailed experiment description). Because the Vela SNR (diameter $\sim 5°$) is considerably larger than the IPC field of view, 36 separate observations were required in order to cover the entire remnant. These are listed in Table 1 (referenced by the *Einstein* sequence number) together with the coordinates of the centers of the fields and the observation durations. The initial survey (sequence numbers in the 700s) left several small gaps at the boundaries of the fields, and a second set of observations (sequence numbers in the 8000s) was performed (mostly in the northeast) to fill in such holes. Several other IPC observations (sequences 2977, 3051, and 6913) were also coincidentally positioned nearby and were used to augment the coverage.

TABLE 1

IPC OBSERVATIONS OF THE VELA SNR

Sequence Number	Image Center α_{1950}	Image Center δ_{1950}	Observing Duration (s)
743.....	$8^h23^m39^s$	$-44°12'$	5469
8034.....	8 26 00	−44 40	2256
738.....	8 26 09	−43 12	2072
8033.....	8 27 00	−43 50	2198
744.....	8 27 15	−45 06	2574
732.....	8 28 34	−42 12	2740
8032.....	8 29 30	−43 20	2007
739.....	8 29 44	−44 05	3134
745.....	8 30 57	−45 59	1515
8030.....	8 32 00	−45 20	2038
8031.....	8 32 00	−44 30	1682
733.....	8 32 08	−43 05	1468
740.....	8 33 25	−44 58	1626
782.....	8 33 36	−45 00	5607
726.....	8 34 27	−42 04	1376
746.....	8 34 47	−46 51	883
734.....	8 35 47	−43 57	4553
2977.....	8 36 12	−42 33	1191
720.....	8 36 41	−41 03	1672
741.....	8 37 13	−45 51	1189
727.....	8 38 05	−42 56	1501
735.....	8 39 34	−44 50	2645
721.....	8 40 18	−41 56	3134
742.....	8 41 08	−46 42	2069
728.....	8 41 49	−43 48	1116
736.....	8 43 27	−45 41	1963
722.....	8 44 01	−42 47	2173
729.....	8 45 41	−44 40	1637
737.....	8 47 27	−46 32	1623
723.....	8 47 50	−43 38	3911
3051.....	8 48 32	−41 54	2401
730.....	8 49 38	−45 31	3364
724.....	8 51 45	−44 29	1710
731.....	8 53 43	−46 21	2603
6913.....	8 54 12	−44 30	1565
725.....	8 55 47	−45 19	2659

In addition to the IPC observations, four observations of the Vela pulsar region were performed with the high resolution imager (HRI), which has a spatial resolution $\sim 4''$. These are discussed in Paper II.

a) The X-Ray Maps

Using the complete set of IPC observations, we compiled X-ray maps of the Vela SNR in two spectral bands: a soft band (0.2–1.0 keV) and a hard band (0.8–2.0 keV). The results are shown in Figures 1*a* and 1*b*. The observed region of sky is outlined in each case. These energy ranges were chosen so as to approximately separate the two components derived by Kahn *et al.* (1983) in their fit to the spectrum of the entire remnant. The energy discrimination is complicated because of low-level gain variations both in time (i.e., between different observations) and as a function of position within the detector. For each field, we determined the average gain and then selected data only from those pulse height bins which, according to this average gain, should primarily sample photons in the desired band. This procedure was later checked after final IPC reprocessing made it possible to gain-correct each individual photon (cf. Harnden *et al.* 1984).

The steps used in constructing the maps were as follows. First, each field was "cleaned" to remove events occurring during periods of high background associated with increased particle flux or with solar X-rays scattered in Earth's atmosphere. An exposure array was constructed for each field which included corrections for telescope vignetting, shadowing by the IPC support ribs, and the effective exposure time. These exposure arrays were then merged to yield a total exposure map summed in $4'.8$ bins. A similar total image map was compiled by merging the individual image arrays, after applying the energy discrimination described above. The ratio of the image map to the exposure map provided the exposure-corrected image of the remnant in each of the two energy bands. The final maps were set to zero in regions where the exposure was less than 10% of the average because of rib shadowing or incomplete coverage. This results in the white "cross-hatching" visible in Figures 1*a* and 1*b*. In assembling the image maps, we made no attempt to subtract background. This was justified since the diffuse emission from the source was observed to exceed the background by at least a factor of 2 at all positions within the remnant. However, since the particle component of the background should not be subject to telescope vignetting, it is possible that we may have overcorrected slightly for vignetting at the edges of the fields. This effect should be small since the particle contribution to the background is minimal at low energies, and although it is barely discernible in the faintest fields, it introduces no qualitative distortion in the overall maps.

As can be seen in Figure 1, the X-ray image of the Vela remnant appears to be roughly oval in shape and extends over 6° in its longest dimension. A well-defined "edge" can be discerned in the north, east, and west, but not in the south. It is clear that our maps are incomplete in that direction, although previous maps constructed from scanning observations suggest that the emission cannot extend more than about 1° further south. We confirm the earlier conclusions that the remnant is brightest in its northwest and southeast quadrants; however, we now find that the enhancements in those directions are associated with smaller, very bright condensations.

The images exhibit a great deal of structure on angular scales ranging from several arcminutes to a few degrees. Most

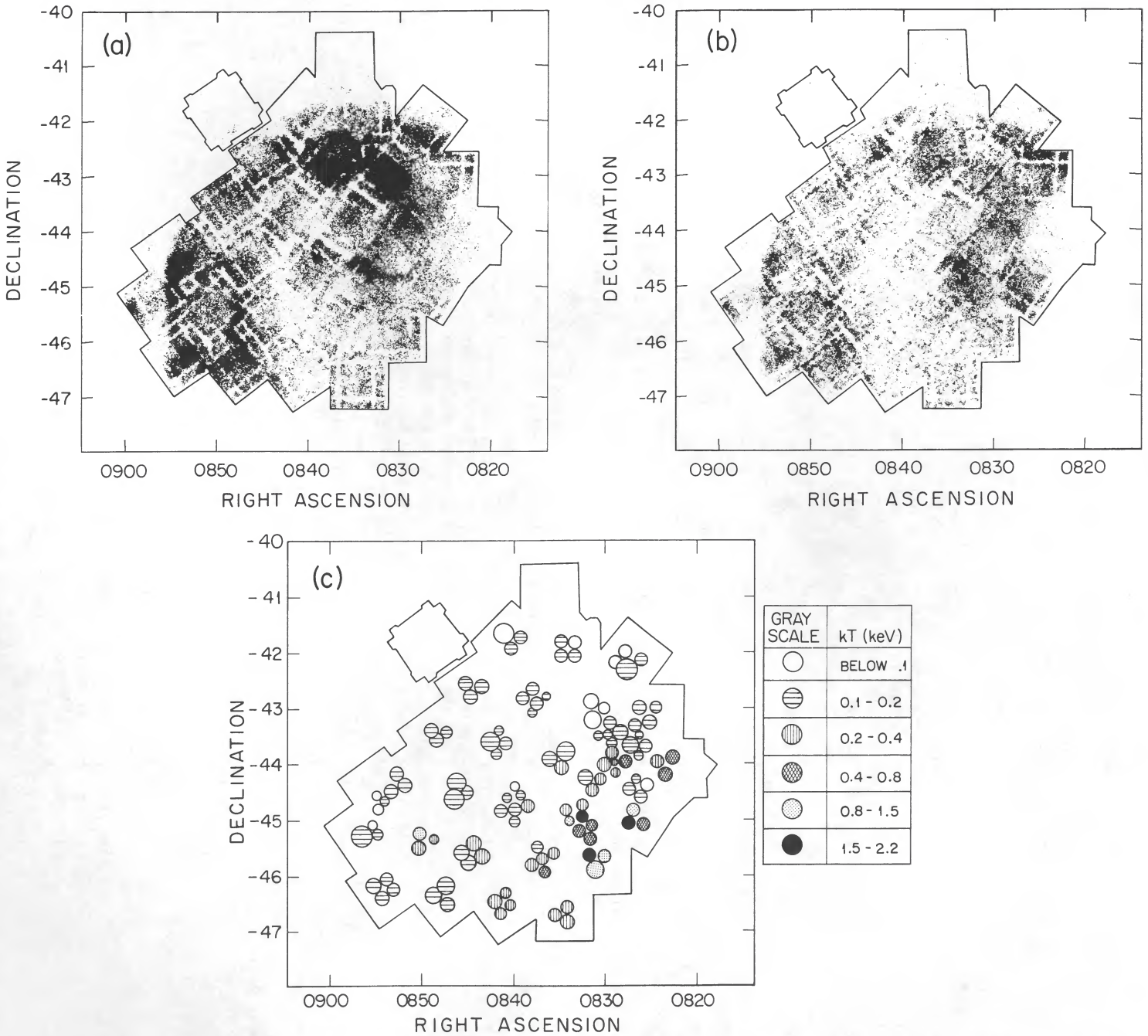

FIG. 1.—(*a*) A map of the Vela SNR in the energy range 0.2–1.0 keV compiled from the *Einstein* IPC observations. The gray scale is linear, with the lowest level set above the mean background level for the fields. The lines mark the outline of the observed region. (*b*) As in (*a*) but for the energy range 0.8–2.0 keV. (*c*) Circular regions in which spectral analysis of the diffuse remnant emission has been performed. The shading indicates best fit temperature as shown.

of this structure is resolved; the only truly unresolved feature is the point source associated with the Vela pulsar at $\alpha = 8^h33^m$, $\delta = -45°$. Items of particular interest include: (1) a prominent shock on the eastern edge at $\alpha = 8^h55^m$; (2) a smaller scale ($\sim 10'$) condensation lying beyond this shock on the eastern edge with a narrow, more diffuse component connecting it back toward the remnant; (3) a bright "cloud," ~ 6–$10'$ in radius, right at the center of the remnant; and (4) narrow filamentary structures (more pronounced in the soft band), one running north-south at $\alpha = 8^h48^m$, and one running east-west at $\delta = -44°.6$. In addition to these discrete features, the maps also both exhibit fainter diffuse emission filling virtually the entire area of the remnant. The gray scales for the images have been adjusted so that the lowest level lies above the background level appropriate to these fields. Thus, essentially all the shading that can be seen in the figures is associated with real X-radiation from the source.

A comparison of Figures 1*a* and 1*b* shows that there are clear spectral variations across the remnant. In order to make these variations more apparent, we have superposed the two maps with different colors. The result is shown in Figure 2*a* (Plate 9). Here, the soft map is plotted in blue and the hard map in red, with full color corresponding, in each case, to the brightest emission observed in the respective energy band. The superposition is such that regions which are considerably softer than average appear blue, regions considerably harder than average appear red, and regions with approximately the same spectrum as the average for the whole remnant appear magenta. A number of interesting conclusions can be drawn from this figure. First, comparison with Figure 1*a* shows that the brightest features in the remnant, such as the central cloud or the condensations in the northwest, are characteristically soft. This is expected if the gas within the remnant is in approximate thermal pressure equilibrium. Second, there appears to be a region of bright, hard X-ray emission ($\sim 1°$ in diameter) to the south of the Vela pulsar. As will be shown in § II*b*, if this emission were thermal, then the emitting gas would have to be considerably overpressured with respect to the rest of the remnant. In Paper II, we demonstrate that the emission is in fact nonthermal synchrotron radiation similar to that found in the Crab Nebula. An additional region of bright, hard emission is found in the extreme northwest. This field lies close to the position of Puppis A, and the emission from that source, which has a considerably harder average spectrum than that of the Vela SNR, is responsible for this feature.

In order to investigate the relationship between the X-ray and optical emission from the remnant, we have superposed the soft map on an [O III] λ5010 filter photograph kindly supplied by T. Gull. This is shown in Figure 2*b* (Plate 9). Here, the soft X-ray emission appears in cyan, and the optical filaments in yellow. Regions which are bright in both bands appear white. The optical photograph has been contrast-enhanced (to suppress stars) so that only the brightest filaments are visible in the picture. The superposition shows that the soft X-radiation is often correlated with the filaments. In particular, the bright cloud at the center of the remnant is coincident with the brightest [O III] filament. Similarly, the soft X-ray extension beyond the shock at the eastern edge lies at the end of a sharp filamentary "wisp." In the northwest, where both the filamentary structure and the X-ray emission are especially pronounced, the filaments appear to outline the bright X-ray regions tightly. This is also observed on the western edge. There are actually two parallel filament lines in the northwest, and both are accompanied by what appear to be irregular X-ray shock fronts. It should be noted, however, that the X-ray/optical correlation is far from complete. In a number of instances (particularly in the south), filaments appear in places devoid of bright X-ray emission.

b) Spectral Analysis

We have derived more quantitative estimates of physical conditions in the X-ray emitting gas by investigating the spectrum of the X-radiation as a function of position within the remnant. The IPC was equipped with 15 pulse height channels nominally spanning the energy range 0.2–4.5 keV. We have extracted pulse height data from a set of circular regions near the centers of the various fields for spectral analysis. The positions of these regions are plotted in Figure 1*c*, which can be compared with Figures 1*a* or 1*b* to infer our spectral coverage across the map.

In order to calibrate detector properties accurately, we have followed the procedures outlined by Fabricant and Gorenstein (1983) (see also Harnden and Fabricant 1985; Charles, Kahn, and McKee 1985): (1) we used background information extracted from regions of deep survey fields which are identical, in detector coordinates, to the regions of the Vela fields; (2) we derived a gain distribution for each region from IPC calibration fields. The background subtraction should be accurate to $\sim 20\%$ of the background count rate, which makes background uncertainties negligible in relation to the count statistics contributions. The systematic uncertainties associated with the calibration of the instrument response are $\sim 3\%$ (cf. Harnden and Fabricant 1985), and these have been added in quadrature to statistical errors in the computation of χ^2 values. Since we are analyzing spectra of diffuse emission, our results are not affected by small-scale gain variations which complicate the analysis of point source spectra.

We have fitted the spectra with a single-component thermal model which incorporates line and continuum emission from an optically thin cosmic abundance plasma in collisional equilibrium (Raymond and Smith 1977; Raymond 1980). Free parameters for the fit are the emission measure, $\mathrm{EM} = \int n_e^2 dl$, the temperature T, and the column density N_H of intervening neutral absorbing material. Use of such a model has been criticized for SNRs because the time scales for equilibrium conditions to be established in the shocked gas (particularly in the ionization structure) can be long compared to the age of the remnant (see Hamilton and Sarazin 1984, and references therein). Nonequilibrium effects should be less pronounced for an intermediate-age remnant like the Vela SNR than for younger remnants but still may be important, particularly in the hotter regions, which are expected to be less dense. Evidence for this is suggested by the fact that the simple equilibrium model provides a better fit to the data in the softer regions, which are generally brighter and thus of higher statistical quality. If the gas is out of equilibrium, then it is usually expected to be underionized, so that the measured temperature is probably lower than the true electron temperature at the respective position within the remnant.

The estimates of T and N_H, derived from the fits, are highly coupled, and we can obtain only weak constraints on either parameter if we allow both to vary freely. As an alternative, then, we may assume that N_H does not vary significantly across the remnant, and require it to lie in the range 1–4×10^{20} cm^{-2}, derived from the fits to the spectrum of the entire remnant by Kahn *et al.* (1983). We believe that this assumption is justified

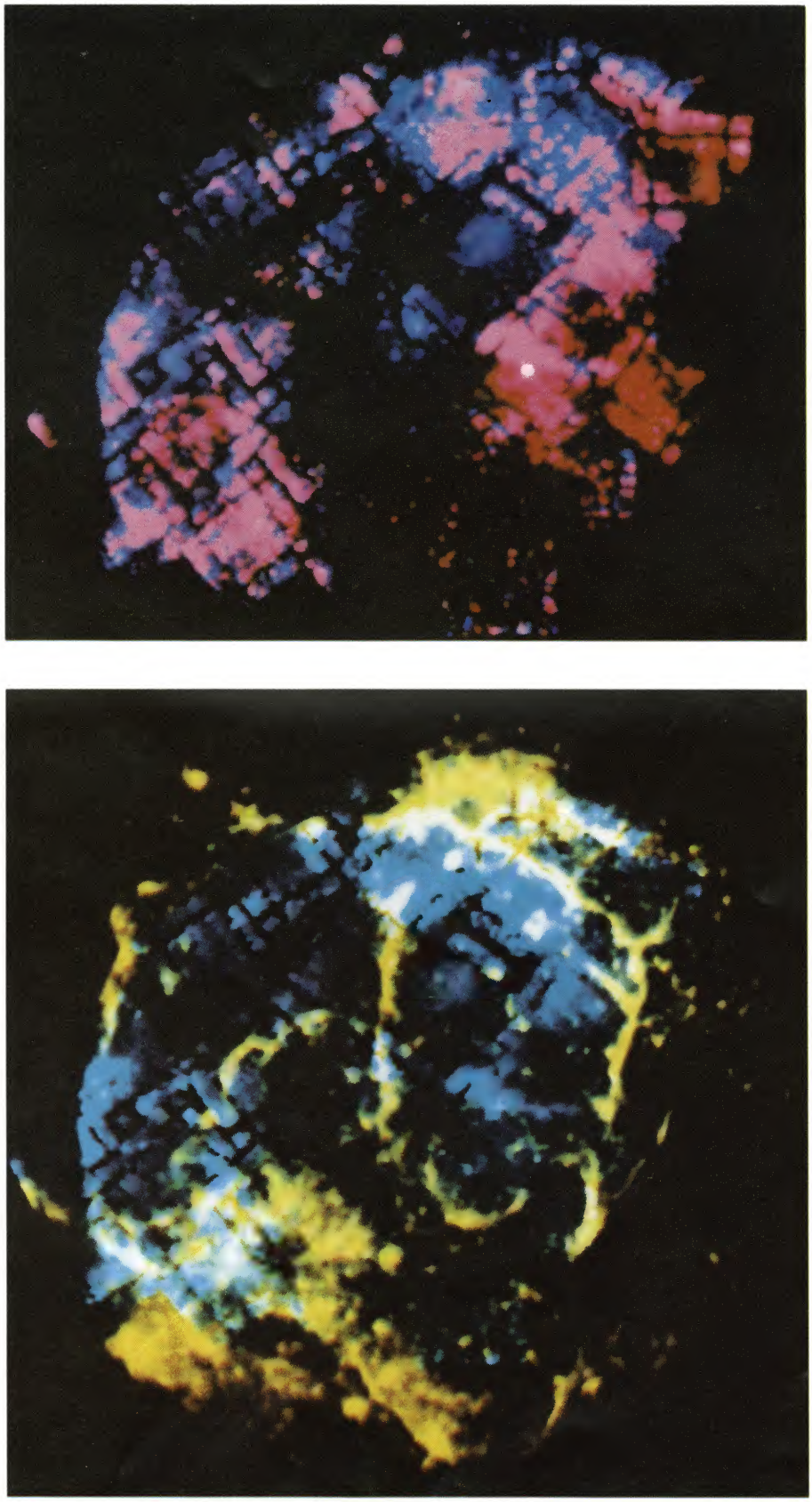

FIG. 2.—(*a*, *top*) An overlay of the maps shown in Figs. 1*a* and 1*b*. The soft map is depicted in blue and the hard map in red. Regions which are bright in both bands appear magenta. (*b*, *bottom*) An overlay of the soft X-ray map of Fig. 1*a* with an [O III] λ5010 filter photograph (Gull 1979). The X-rays appear in cyan and the optical in yellow. Regions which are bright in both bands appear white.

for two reasons: (1) The data from all the individual regions are consistent with N_H lying in this range; i.e., we see no evidence of absorption variations. (2) If N_H varied substantially more than this, Kahn *et al.* (1983) could have deduced it from their spectrum of the entire remnant. Their data would not have been consistent with a model involving uniform absorption but would have required "leaky absorption," which exhibits a much flatter energy dependence.

Having restricted N_H in this way, we were then able to derive relatively tight constraints on the temperature. In Figure 1*c* we have shaded each of the regions with a gray level indicating the best fit temperature. As can be seen, the spectral fitting confirms the conclusions drawn from Figure 2*a*. The brightest regions of the remnant are quite soft, with best fit temperatures below 10^6 K. The area surrounding the Vela pulsar is quite hard, with best fit temperatures ~ 2–3×10^7 K (see Paper II).

In Figure 3, we have plotted 99% confidence regions in EM versus T space for a representative sample of the regions selected for spectral analysis. Several conclusions can be drawn from this figure. (1) The contours are not all mutually consistent. Statistically significant scatter is observed in the derived temperature, which confirms the spectral variations inferred from Figures 2*a* and 1*c*. For regions which do exhibit the same spectral shape, we also observe statistically significant variations in the derived emission measure. (2) The emission measure appears to decrease monotonically with increasing temperature. The individual contours themselves show such a trend, since the best fit values of EM and T are coupled. However, the anticorrelation holds for contours which are not overlapping, which proves that the effect is real. (3) At the high-temperature end, $T > 10^7$ K, there is a group of contours which also lie at higher values of EM. All these contours are in fact associated with regions in the vicinity of the Vela pulsar.

If the gas within the remnant is in thermal pressure equilibrium, then one expects the anticorrelation between EM and T noted above: EM $\propto n_e^2 \propto T^{-2}$. However, EM also depends on the line-of-sight extent of the emitting gas l, which almost certainly varies across the remnant. This is probably responsible for the observed variations in emission measure seen for regions which exhibit the same mean temperature. In order to derive an estimate of the pressure, we may use the upper envelope of the observed distribution and assume that this corresponds to the set of regions for which l is approximately the diameter of the remnant, ~ 40 pc. A dashed line obeying EM $\propto T^{-2}$, which appears to describe the upper envelope, is shown in Figure 3. The implied pressure is $p/k \approx 3.5 \times 10^5$ cm^{-3} K, where k is Boltzmann's constant. If the maximum value of l is less than the diameter of the remnant, then the pressure may be higher, but probably not by more than $\sim 50\%$. It is of interest that this derived value of the pressure agrees rather well with previous estimates based on the integrated spectrum and luminosity of the entire remnant (cf. Tucker 1971).

Note that the contours at higher temperatures associated with the vicinity of the Vela pulsar lie well above the extrapolation of the pressure equilibrium line. Since such severe variations in gas pressure are not expected to persist within the remnant, it seems likely that the emission in these regions is nonthermal, as discussed in Paper II. Nonequilibrium effects would only make the problem worse, since the measured temperature would then be a lower limit to the true electron temperature.

III. DISCUSSION

The observations of the Vela SNR with the *Einstein* IPC have demonstrated explicitly the intricacy and complexity of the X-ray emission from this remnant. Our derived map exhibits spectral and intensity variations on scales ranging from one to tens of parsecs. The emission is highly asymmetric and inhomogeneous, with bright regions distributed irregularly across the region. This contrasts dramatically with the symmetric "limb-brightened shell" appearance of the X-ray image of the Cygnus Loop (Ku *et al.* 1984) and thus further

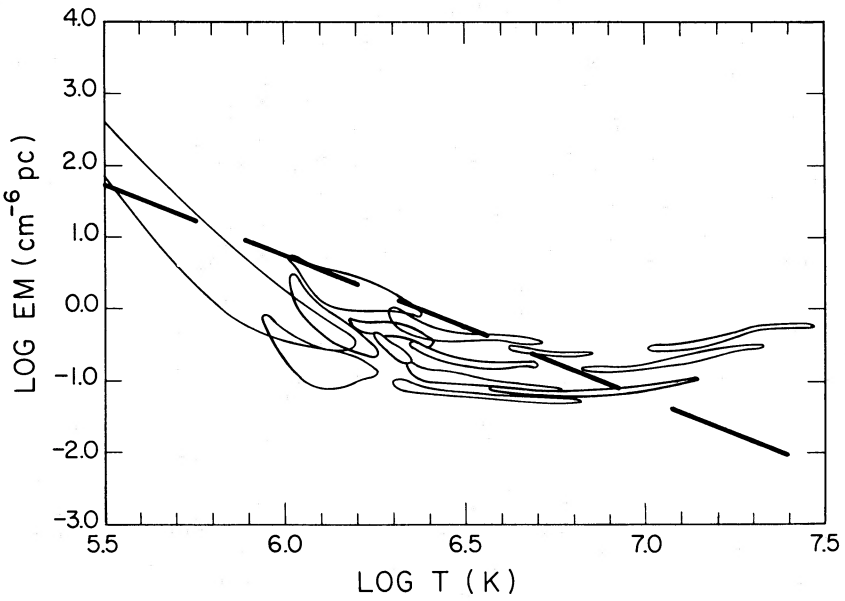

FIG. 3.—A sample of 99% confidence regions in EM vs. T space for various circular regions within the remnant selected for spectral analysis (see text). The contours plotted span the range of those derived from the spectral fits. The dashed line has the form EM $\propto T^{-2}$, as expected if the remnant is in approximate pressure equilibrium. Note that it appears to describe the upper envelope of the measured distribution.

emphasizes the distinction between these two intermediate-age remnants.

The X-radiation from Vela appears to be thermal in origin, with the exception of a $\sim 1°$ region of hard X-ray emission in the vicinity of the Vela pulsar. Our spectral analysis shows that there are substantial temperature variations across the remnant. We find that the emission is consistent with the gas being roughly in thermal pressure equilibrium, although pressure variations by as large as a factor 10 cannot be ruled out by our observations. The softest and brightest X-ray emission shows a marked association with the bright [O III] filaments; however, this correlation is far from exact. In some cases, the bright filaments are surrounded by X-ray enhancements, while in others, the filaments appear to outline the X-ray emission. In the standard picture, these bright optical and ultraviolet filaments are thought to be produced by slower shocks driven into denser clouds which have been overtaken by the blast wave (McKee and Cowie 1975). The soft X-ray emission, which is associated with the filaments, might then originate in gas of intermediate density located near the clouds. This intermediate gas may have been present prior to the passage of the shock, or may have been produced by evaporation of the cloud material due to thermal conduction from the shocked hot intercloud medium (Cowie and McKee 1977; McKee and Cowie 1977). Below we evaluate such a scenario quantitatively.

We concentrate on the small cloud at the center of the remnant ($\alpha = 08^h39^m$, $\delta = -44°30'$), for which the coincidence of bright soft X-ray emission and [O III] emission is particularly clear (see Fig. 2*b*). This cloud has been observed with the *International Ultraviolet Explorer* (*IUE*) by Raymond *et al.* (1981). They find that the relative intensities of the ultraviolet lines agree reasonably well with models of radiative, planar shocks characterized by shock velocities $\sim 132 \pm 5$ km s^{-1}. If such a shock is associated with the cloud's having been overtaken by the SNR blast wave, then the analysis of McKee and Cowie (1975) shows that

$$\rho_c v_c^2 \approx F p_i , \tag{1}$$

assuming that the cloud shock is approximately isothermal. Here ρ_c is the preshock mass density of the cloud, v_c is the velocity of the cloud shock, p_i is the ambient pressure in the hot intercloud medium behind the blast wave, and F is the ratio of the pressure behind the cloud shock to the pressure behind the bow shock in the intercloud gas. The quantity F depends on the Mach number of the intercloud flow with respect to the cloud. If the cloud has been shocked very recently, then F can be as high as 2.1 (for parameters appropriate to the Vela SNR), and p_i should be of order twice the measured average pressure in the remnant, $\langle p \rangle$. If the cloud was overtaken much earlier, then $F \approx 1$, $p_i \approx \langle p \rangle$. Using our measured value for $\langle p \rangle$ and the value of v_c inferred from the *IUE* observations, we find that the preshock density of the cloud is constrained to lie in the range

$$0.14 \leq n_c \leq 0.64 \text{ cm}^{-3} . \tag{2}$$

This density estimate can be compared to that obtained by looking at the intensity of the ultraviolet emission lines. [O III] $\lambda 1663$ is a good line to use, since it is bright and should be unattenuated within the cloud. Raymond *et al.* (1981) measure an intensity of 8.4×10^{-5} ergs cm^{-2} s^{-1} sr^{-1} for this line. The predicted intensity, looking face on to the shock, is given by Shull and McKee (1979) for a shock model with $n_c = 10$ cm^{-3}, $v_c = 130$ km s^{-1}: $I(\lambda 1663) = 1.33 \times 10^{-5}$ ergs cm^{-2} s^{-1} sr^{-1}. The intensity should scale linearly with n_c, since the cooling time is inversely proportional to n_c (McCray and Snow 1979). The inferred density estimate for the cloud is then

$$n_c = 63 f^{-1} \text{ cm}^{-3} , \tag{3}$$

where f is the ratio of the extent of the shock along our line of sight to the cooling length behind the shock. Comparison with inequality (2) would require $f \geq 100$, which seems extremely unlikely even though this is one of the brighter and narrower filaments in the remnant. An additional check on the density comes from the requirement that the cloud shock be radiative, i.e., that the cooling time for gas behind the shock not exceed either the age of the remnant or the time scale for the shock to cross the cloud. The age of the Vela SNR is ~ 1–2×10^4 yr and the cloud crossing time is $\sim 10^4$ yr. Using the expression given in McKee and Cowie (1975), we calculate a range in cooling time of 0.2–1 $\times 10^4$ yr, with the lowest values corresponding to the highest allowed densities. Thus the cloud shock is only marginally radiative even for the highest values of n_c allowed by the dynamical argument.

Further problems are encountered if we quantitatively evaluate the soft X-ray emission associated with this cloud. Our spectral fits in this region imply an allowed temperature range of 1.0–1.9 $\times 10^6$ K and an emission measure range of 0.46–3.0 cm^{-6} pc. The highest temperature and lowest emission measure values are required if the cloud is in near pressure equilibrium with the hotter regions in the remnant. The cloud has an apparent size ~ 1 pc in the plane of the sky. Even if it is "flattened" in the direction perpendicular to the shock face, and if the shock is highly inclined to the line of sight, it is likely that the line-of-sight extent of the cloud is ≤ 5 pc. That implies a density 0.3 cm^{-3} or greater for the soft X-ray emitting gas. This density estimate is not small compared to the estimates of the preshock density of the cloud given by inequality (2). If the soft X-rays are produced by evaporating gas, then this would imply that a major fraction of the cloud must have already evaporated for this picture to be consistent. Following the analysis of Cowie and McKee (1977), we estimate an evaporation time scale for the cloud $\sim 10^4$ yr, so such an interpretation is somewhat implausible.

The discussion above shows that the "standard" picture of SNR propagation in a cloudy medium is only marginally consistent with our observations. Virtually all the problems, however, can be reconciled if our derived value of the dynamic pressure which drives a shock in the cloud is an underestimate. This is possible if the maximum line of sight extent of emitting gas is much less than the remnant diameter, although that interpretation appears to conflict with the appearance of the remnant in the plane of the sky. Another possibility is that the particular cloud we are investigating was overshocked due to an encounter with expanding ejecta from the initial explosion. Finally, although unlikely, it is possible that the pressure associated with magnetic fields and with relativistic particles is dominant over the gas pressure at the shock face. In that case, the derived preshock cloud density might be larger by a factor of a few.

Because [O III] $\lambda 5007$ and $\lambda 1663$ are only produced in high-velocity shocks (> 100 km s^{-1}), the [O III] filaments are likely, in any case, to be associated with the lower density phase of the cloud component. High-density concentrations would be more prominent in lower excitation lines like Hα, Hβ, and [S II]

λ6731. Maps of the Vela SNR in these lines have been published by Parker, Gull, and Kirschner (1979). The filaments are generally less pronounced in these maps, and lower level diffuse emission appears in regions bounded by the sharp [O III] filaments, particularly in the northwest. That suggests that the lower density gas which shows up brightly in [O III] may be a "fringe" to higher density concentrations. Such a conclusion is supported by the absorption line studies of Jenkins, Wallerstein, and Silk (1984). They found two stars with unusually strong interstellar absorption lines of excited neutral carbon, which are indicative of dense neutral clouds at pressures comparable to that of the X-ray–emitting gas in the Vela SNR. Both these stars lie behind the remnant in the northwest, in an area bounded by prominent [O III] filaments. If the brightest, softest X-ray emission is associated with gas evaporating from dense clouds, then one expects to see soft X-ray enhancements near such dense concentrations as well. This may explain why the [O III] filaments appear to outline some of the brightest X-ray regions.

If the evaporation of dense clouds is indeed prevalent in the Vela SNR, then it may affect the dynamics of the remnant. McKee and Ostriker (1977) find, for example, that for an evaporative remnant, the radius evolves as $t^{3/5}$ (where t is the age), as opposed to the standard Sedov law, $R \propto t^{2/5}$. They also find that the X-ray appearance should be significantly less limb-brightened than for a Sedov remnant. It is interesting to note that our X-ray image of the Vela SNR does not show prominent limb brightening except on the eastern edge. The evolution may therefore have been evaporation-dominated. However, it is difficult to draw strong conclusions in this regard, since the image is quite asymmetric in many respects. Other, considerably younger remnants also fail to show *complete* limb-brightened shells.

We are left with the question of why the Vela and Cygnus Loop SNRs exhibit such different morphological structure. Much of the spatial complexity of the Vela image can be understood as a natural consequence of a remnant evolving into a very nonuniform interstellar medium. The relevant issue may therefore be, "Why is the Cygnus Loop so symmetric?" instead of, "Why is the Vela SNR so complex?" McCray and Snow (1979) have suggested that the ambient medium surrounding the Cygnus Loop supernova may have been "homogenized" by a strong stellar wind emanating from an early-type progenitor star (see also Charles, Kahn, and McKee 1985). Perhaps the Vela progenitor star was of later spectral type or had an anomalously weak wind, so that the medium was left nonuniform in that case. Clearly, further research along these lines will be necessary to clarify such issues. Detailed X-ray images of older SNRs in nearby galaxies would be particularly useful in this regard.

We acknowledge Karl Citek of the Columbia Astrophysics Laboratory for extensive help with the data analysis, and Ted Gull for the use of his optical picture prior to publication. The authors also wish to thank Chris McKee, John Raymond, and Jack Hughes for several useful discussions. This work was supported by NASA under contracts NAS8-30751 and NAS8-30753.

REFERENCES

Charles, P. A., Kahn, S. M., and McKee, C. F. 1985, *Ap. J.*, **295**, 456.
Cowie, L. L., and McKee, C. F. 1977, *Ap. J.*, **211**, 135.
Culhane, J. L. 1977, in *Supernovae*, ed. D. N. Schramm (Dordrecht: Reidel), p. 29.
Culhane, J. L., Cruise, A. M., Rapley, C. G., and Hawkins, F. J. 1974, *Ap. J. (Letters)*, **190**, L9.
Fabricant, D., and Gorenstein, P. 1983, *Ap. J.*, **267**, 535.
Giacconi, R., *et al.* 1979, *Ap. J.*, **230**, 540.
Gorenstein, P., Harnden, F. R., Jr., and Fabricant, D. G. 1981, *IEEE Trans*, **NS-28**, 869.
Gorenstein, P., Harnden, F. R., Jr., and Tucker, W. H. 1974, *Ap. J.*, **192**, 661.
Gull, T. 1979, private communication.
Hamilton, A. J. S., and Sarazin, C. L. 1984, *Ap. J.*, **284**, 601.
Harnden, F. R., Jr., and Fabricant, D. G. 1985, in preparation.
Harnden, F. R., Jr., Fabricant, D. G., Harris, D. E., and Schwarz, J. 1984, *Smithsonian Ap. Obs., Spec. Rept.*, No. 393.
Harnden, F. R., Jr., and Gorenstein, P. 1973, *Nature*, **241**, 107.
Harnden, F. R., Jr., Grant, P. D., Seward, F. D., and Kahn, S. M. 1985, *Ap. J.*, **299**, 828 (Paper II).
Hearn, D. R., Larsen, S. E., and Richardson, J. A. 1980, *Ap. J. (Letters)*, **235**, L67.
Jenkins, E. B., Wallerstein, G., and Silk, J. 1984, *Ap. J.*, **278**, 649.
Kahn, S. M., Brodie, J., Bowyer, S., and Charles, P. A. 1983, *Ap. J.*, **269**, 212.
Kellogg, E., Tananbaum, H., Harnden, F. R., Jr., Gursky, H., and Giacconi, R. 1973, *Ap. J.*, **183**, 935.
Ku, W. H.-M., Kahn, S. M., Pisarski, R., and Long, K. S. 1984, *Ap. J.*, **278**, 615.
McCray, R., and Snow, T. P. 1979, *Ann. Rev. Astr. Ap.*, **17**, 213.
McKee, C. F., and Cowie, L. L. 1975, *Ap. J.*, **195**, 715.
———. 1977, *Ap. J.*, **215**, 213.
McKee, C. F., and Ostriker, J. P. 1977, *Ap. J.*, **218**, 148.
Miller, E. W. 1973, *Pub. A.S.P.*, **85**, 764.
Moore, W. E., and Garmire, G. P. 1975, *Ap. J.*, **199**, 680.
Parker, R. A. R., Gull, T. R., and Kirschner, R. P. 1979, *An Emission-Line Survey of the Milky Way* (Washington, D. C.: NASA Science and Technical Information Branch).
Raymond, J. C. 1980, private communication.
Raymond, J. C., Black, J. H., Dupree, A. K., Hartmann, L., and Wolff, R. S. 1981, *Ap. J.*, **246**, 100.
Raymond, J. C., and Smith, B. W. 1977, *Ap. J. Suppl.*, **35**, 419.
Seward, F. D., Burginyon, G. A., Grader, R. J., Hill, R. W., Palmieri, T. M., and Stoering, J. P. 1971, *Ap. J.*, **169**, 515.
Shull, J. M., and McKee, C. F. 1979, *Ap. J.*, **227**, 131.
Tucker, W. H. 1971, *Ap. J. (Letters)*, **167**, L85.
van den Bergh, S. 1978, *Ap. J. Suppl.*, **38**, 119.

P. GORENSTEIN, F. R. HARNDEN, JR., and F. D. SEWARD: Harvard-Smithsonian Center for Astrophysics, 60 Garden Street, Cambridge, MA 02138

STEVEN M. KAHN: Department of Physics, University of California, Berkeley, CA 94720